Research Square

Preprints are preliminary reports that have not undergone peer review.
They should not be considered conclusive, used to inform clinical practice,
or referenced by the media as validated information.

Chemical-Vapour-Deposition Diamond as the Primary Product and as a Chemical Clock of a Near-Light-Speed Energy-Sheath Apparatus: Yields, Uses, and a Test of the Börekci Metric

Hasan Börekci

hborekci@hotmail.com.tr

HB ZECHMANN Medical Company

Research Article

Keywords: CVD diamond, chemical clock, gravitational time dilation, Börekci metric, energy sheath, positron production

Posted Date: September 15th, 2026

DOI: https://doi.org/10.21203/rs.3.rs-10844462/v1

License: This work is licensed under a Creative Commons Attribution 4.0 International License.
Read Full License

Additional Declarations: No competing interests reported.

Chemical-Vapour-Deposition Diamond as the Primary Product and as a Chemical Clock of a Near-Light-Speed Energy-Sheath Apparatus: Yields, Uses, and a Test of the Börekci Metric

Hasan Börekci[1,*]

[1] R&D Directory, HB ZECHMANN Medical Company, Manisa Technopark, Celal Bayar University Area, Manisa, Türkiye (Assistant Professor of General Surgery; independent theoretical physics researcher)

* Corresponding author: hborekci@hotmail.com.tr — ORCID 0000-0001-9137-6342

Abstract

We describe an apparatus (BEF-2026) in which a stationary ellipsoidal capsule is completely enclosed, from pole to pole, by a co-propagating sheath of 25 MeV electrons and 20 kW laser light, and we show that its most robust product is chemical-vapour-deposition (CVD) diamond. A 0.2 atm CH_4/H_2 jet, dissociated by the 25 MeV beam and by the white-hot (≈ 2,302 K) tungsten–rhenium anode, grows polycrystalline diamond on two 1 m^2 substrate sets, one inside and one outside the sheath enclosure, at ≈ 253 g per set per 24 h (2,527 carats in total), and single-crystal gem material on 1,000 seed plates at ≈ 413 carats of rough per day. We explain why pure carbon vapour cannot give diamond and why the product is needed industrially (heat spreaders, laser windows, electrodes, detectors) and for jewellery. The apparatus was proposed to test whether an enclosing near-light-speed energy flow modifies the interior metric; we formulate this as the Börekci metric, in which one parameter ξ multiplies the sheath potential and $\xi = 1$ recovers linearised general relativity. General relativity predicts a sheath-induced clock offset of -1.27×10^{-47}; the author's conjecture (interior Lorentz factor equal to that of the electrons, 49.9) requires $\xi \approx 3.9\times10^{46}$. The two substrate sets act as a chemical clock: their thickness ratio equals $1/\Gamma_{in}$, so a ratio resolution of 10^{-3} bounds $\xi < 7.8\times10^{43}$, while the conjecture predicts a ratio of 0.020. Positron production (≈ 2.5×10^{19} e^+ per day) is summarised. All results are given in both frameworks so that the experiment, not the text, decides.

Keywords: CVD diamond; chemical clock; gravitational time dilation; Börekci metric; energy sheath; positron production

1 Introduction

Most proposals to test general relativity in the laboratory measure a clock. This paper describes an apparatus whose most reliable output is not a clock reading but a material: diamond grown by chemical vapour deposition (CVD) in the gap between two concentric capsules, one of which is wrapped by a near-light-speed sheath of electrons and laser light. The apparatus — the Börekci Energy Field, BEF-2026 — was conceived to test a conjecture about spacetime: that a stationary volume completely enclosed by an energy flow moving at nearly the speed of light acquires, by the principle of relativity, the time dilation of the flow itself [1]. Standard general relativity predicts otherwise, and the two predictions differ by forty-six orders of magnitude in a single parameter. What makes the diamond more than a by-product is that its growth is a clock: a film grown inside the enclosure and a film grown outside it must have the same thickness if general relativity is right, and thicknesses differing by a factor of fifty if the conjecture is right. The diamond therefore carries both the economic and the epistemic weight of the experiment.

Three questions organise the paper. First, what does the apparatus actually make, in what quantities, and why is that product needed — industrially and for jewellery (Sections 2–3)? Second, what does the modified metric that motivated the apparatus predict, stated briefly and in a form that reduces to general relativity when the new parameter is set to unity (Section 4)? Third, how does the diamond yield itself depend on

that parameter, i.e. how does the film work as a chemical clock (Section 5)? Antimatter production, the original selling point of the design, is summarised in Section 6 because its economic value turns out to be negligible next to the diamond, although the positron flux is world-class. Throughout, results are given in two frameworks: standard general relativity ($\xi = 1$) and the author's conjecture ($\xi \gg 1$). The author states his conviction openly and the standard theory is stated with equal clarity; the two are separated by measurement, not by rhetoric.

The conceptual novelty offered to this journal is modest and precise: a linearised metric with one coupling parameter attached to the energy–momentum of a null-like enclosing flow, a demonstration that the parameter is bounded by clocks and by a material-growth ratio alike, and the observation that a diamond film — a chemical process integrating over proper time — is a legitimate, electronics-free clock for such a test. The engineering, radiological and economic details of the full apparatus are given in a companion technical report [1] and are only summarised here.

Relation to the author's other work on BEF-2026. In the interest of full transparency, and to forestall any concern about redundant or salami-type publication, the author discloses that the same apparatus has been described from several distinct angles. A companion preprint treats the full apparatus as a positron source and candidate time-dilation capsule, with the detailed engineering, radiological and safety analysis [1]; the author additionally maintains a small number of related preprints on the Zenodo and Research Square repositories that address other aspects of the same research programme. The present manuscript is self-contained and does not reproduce the results of those works. Its distinct and, to the author's knowledge, previously unreported contributions are the CVD-diamond yield analysis of Sections 3 and 5, the industrial and jewellery use case, and the diamond-film chemical-clock method for bounding the metric parameter ξ. The material that necessarily overlaps — the apparatus description (Section 2) and the metric (Section 4) — is deliberately condensed and cross-referenced to the companion report rather than restated in full, and where an earlier numerical result of that report is superseded (notably the positron yield) this is stated explicitly (Section 6). The author will gladly provide the editors with the full list of related preprints and welcomes guidance if any further separation is required.

2 The Apparatus in Brief

Figure 1 shows a scaled meridional section and Table 1 the principal parameters. The outer capsule is a sphere of 16.0 m free inner diameter whose wall, from outside inwards, consists of a borosilicate skin, 150 cm of SiC/SiC ceramic-matrix composite (density ≈ 2.65 g cm^{-3}, service temperature > 1400 °C [2]), 50 cm of circulating water and 90 cm of tungsten–steel composite; the gap inside it is evacuated. At its centre stands a prolate ellipsoidal inner capsule, 12.0 m pole to pole and 10.0 m at the equator, with walls of 90 cm SiC/SiC, 90 cm tungsten–steel, 100 cm lead and 30 cm water enclosing a cavity of 43.9 m^3 of air at 1 atm; a pair of 2 T superconducting magnets at the cavity's poles provides a dipole field whose lines wrap the capsule in the gap. Just outside the two poles sit solid tungsten–rhenium electrodes (10 cm diameter, 20 cm long; melting point 3120 °C [3]), rotating at 700 rpm and vibrating at 100 Hz. A potential of 25 MV between them drives an electron sheath (50–200 µA at start, 0.5–2 mA in steady operation) that flows from the top pole around the capsule into the bottom anode; a co-propagating 20 kW continuous-wave ring laser follows the same meridians. The electrons have $\gamma_e = 49.92$; at 2 mA there are 7.9×10^8 electrons in flight at any instant, carrying 3.2 mJ in a sheath whose density (6.1 cm^{-3}) is that of the solar wind. The apparatus is housed in a sealed cavern under a mountain and runs for 24 h per cycle.

Two design corrections adopted from the technical audit are relevant here. The masses computed from the wall thicknesses are 16,930 t for the outer and 4,458 t for the inner capsule (not the 150 t and 90 t of the first draft), and the gas injected at the bottom pole is not pure carbon vapour but a 2–5 vol.% CH_4/H_2 mixture at 0.2 atm (Section 3.1). Open engineering items — transport of the electron sheath around the

capsule, holding 25 MV across a 2–4 m vacuum gap, cooling of the rotating anode and mechanical support of the inner capsule — are listed in the technical report and do not affect the diamond chemistry, which takes place in the anode region and on the capsule skin.

Figure 1. BEF-2026 apparatus — vertical (meridional) section, to scale (metres)

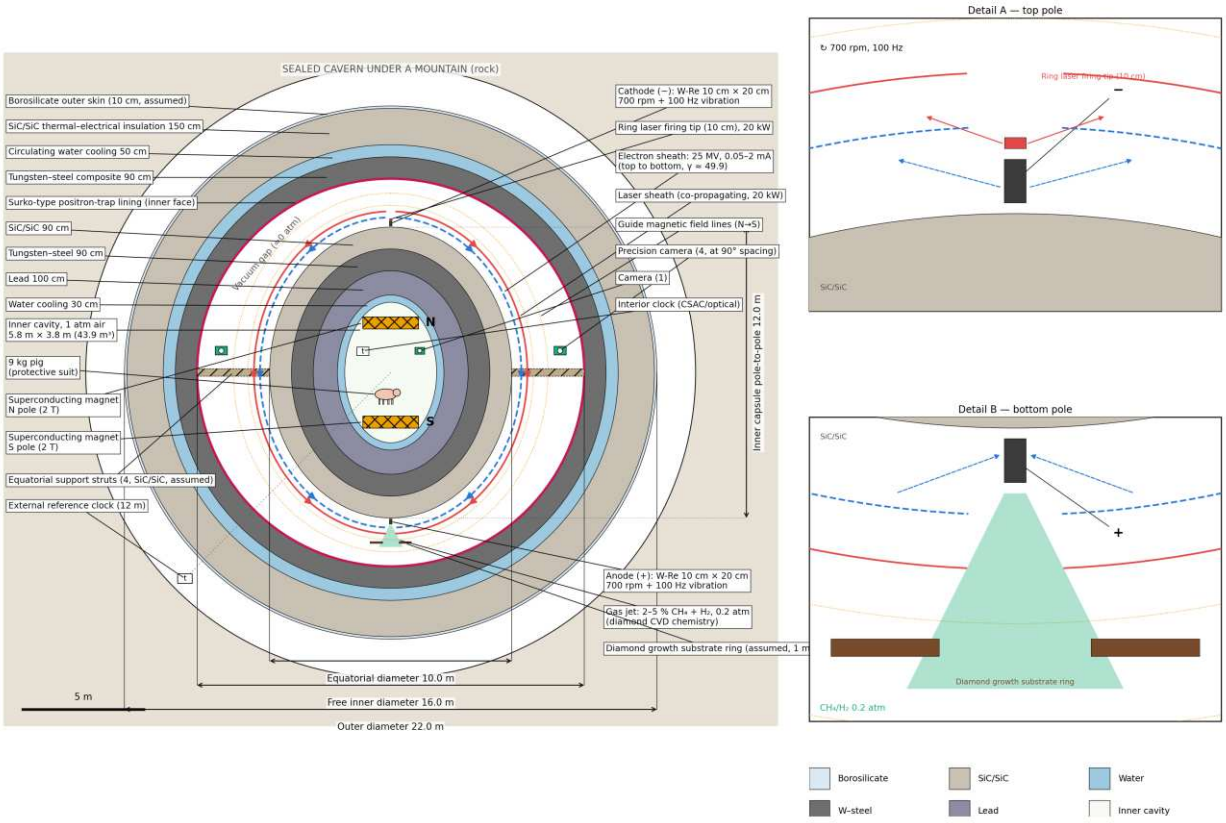


Fig. 1 Scaled meridional section of the BEF-2026 apparatus: outer sphere (16 m free inner diameter; borosilicate, SiC/SiC 150 cm, water 50 cm, tungsten–steel 90 cm, positron-trap lining), inner ellipsoidal capsule (12 m × 10 m; SiC/SiC 90 cm, tungsten–steel 90 cm, lead 100 cm, water 30 cm), the 2 T magnet pair, the W-Re electrodes at the poles, the electron (blue dashed) and laser (red) sheaths, the guide field lines (orange dotted), the CH_4/H_2 gas jet and the diamond substrate ring at the bottom pole. Details A and B enlarge the pole regions. The equatorial struts are an assumption of the design audit.

Table 1 Principal parameters of BEF-2026 (values from the calculation model, Online Resource 1).

Subsystem	Specification	Derived quantity
Outer capsule	sphere, 16.0 m free ID; borosilicate / SiC/SiC 150 cm / water 50 cm / W–steel 90 cm; vacuum inside	mass ≈ 16,930 t; outer diameter 22.0 m
Inner capsule	prolate ellipsoid 12.0 × 10.0 m; SiC/SiC 90 cm / W–steel 90 cm / Pb 100 cm / water 30 cm; 1 atm air inside	mass ≈ 4,458 t; cavity 5.8 × 3.8 m (43.9 m^3)
Magnets	2 T superconducting pair at cavity poles (N up, S down)	stored energy ≈ 140 MJ; gap field ≈ 0.1–0.2 T
Electrodes	W–Re, Ø 10 cm × 20 cm, 700 rpm, 100 Hz vibration; cathode top, anode bottom	rim speed 3.67 m/s; anode radiative equilibrium ≈ 2,302 K at 50 kW
Electron sheath	25 MV; 50–200 µA start, 0.5–2 mA steady; pole-to-pole path 18.9 m	γ_e = 49.92; 7.9×10^8 e^- in flight; 3.2 mJ; 6.1 cm^{-3}
Laser	20 kW CW ring laser, co-propagating	1.26 mJ in flight; 1.73×10^9 J per 24 h
Gas jet	2–5 % CH_4 in H_2, 0.2 atm (152 Torr), local to the anode	electron energy loss 8 keV per pass
Diamond substrates	set A: 1 m^2 on the inner-capsule skin (inside the sheath); set B: 1 m^2 on the outer wall (outside); 1,000 single-crystal seeds 7 × 7 mm	see Table 2

Subsystem	Specification	Derived quantity
Positron-trap lining	moderator-coated inner face of the outer wall + 100 Surko-type traps	see Table 6
Run	24 h; magnet ramped 2 h before; arc, laser and jet fired simultaneously at t = 0	beam energy 1,200 kWh; total site power ≈ 400 kW

3 Diamond Growth in the Apparatus

3.1 Chemistry: why carbon vapour fails and what the CH_{4}/H_{2} jet does

The first draft of the design injected carbon vapour at 0.2 atm from the anode. This cannot produce diamond. Carbon sublimates at ≈ 3900 K at 1 atm and still needs ≈ 3650 K at 0.2 atm; between water-cooled walls the vapour condenses at once, and what condenses is soot, amorphous carbon and fullerenes — the product of the Krätschmer–Huffman arc, in which graphite is evaporated in 100–200 Torr of helium [4]. Diamond is metastable at ambient pressure. Its growth at low pressure relies on a kinetic trick discovered in the 1980s: atomic hydrogen etches sp^2 (graphitic) carbon about fifty times faster than diamond, so that on a substrate held at 700–1000 °C only the diamond phase survives [5]. The jet was therefore redefined as 2–5 vol.% CH_4 in H_2 at 0.2 atm (152 Torr), inside the 100–300 Torr window of microwave-plasma CVD reactors [6].

The apparatus supplies the atomic hydrogen in two ways. The anode absorbs the full 50 kW of the beam; without forced cooling its radiative equilibrium temperature is ≈ 2,302 K, i.e. it is a hot-filament CVD source of exactly the kind (tungsten at 2000–2400 °C) used in hot-filament reactors, and the 25 MeV electrons ionise and dissociate the gas along their path (energy loss 8 keV per pass through a 1 m jet, negligible for the beam, large for the gas). The electron and laser sheath, which is transparent to the gas, adds ultraviolet and X-ray photolysis. The substrates must be kept out of the direct beam, because 25 MeV electrons displace carbon atoms in the lattice; they are mounted on the inner-capsule skin at mid-latitude (set A, inside the sheath enclosure) and on the outer wall at the same height (set B, outside it), both at 850–950 °C, both fed by the same gas.

3.2 Yields

For polycrystalline film the growth rate of hot-filament and plasma reactors is 1–10 µm h^{-1}; we take 3 µm h^{-1} as the nominal value. Each 1 m^2 set then grows 72 µm in 24 h, i.e. 253 g (ρ = 3.51 g cm^{-3}), and the two sets together 505 g or 2,527 carats of thermal-grade material per cycle. Single-crystal (homoepitaxial) growth on seed plates is the route to gem material. With 1,000 seeds of 7 × 7 mm and a rate of 20 µm h^{-1} — the record rate with nitrogen addition is 50–150 µm h^{-1} [7], but colourless material grows more slowly [6] — one cycle deposits 83 g, i.e. 413 carats of single-crystal rough, which polishes to ≈ 165 carats (40 % yield). A polished 1 ct stone needs a crystal ≈ 3.5 mm thick, i.e. ≈ 7.3 consecutive cycles on the same seed; the apparatus is therefore run in multi-day campaigns for gems and in single cycles for film.

$$m_{\mathrm{diamond}} = A_{\mathrm{substrate}}\, r\, t_{\mathrm{run}}\, \rho_{\mathrm{diamond}} \tag{1}$$

$$m_{\mathrm{sc}} = N_{\mathrm{seed}}\, A_{\mathrm{seed}}\, r_{\mathrm{sc}}\, t_{\mathrm{run}}\, \rho_{\mathrm{diamond}}, \qquad N_{\mathrm{carat}} = 5000\, m_{\mathrm{sc}}[\mathrm{kg}] \tag{2}$$

Table 2 Diamond yields per 24 h cycle at ξ = 1 (general relativity). Prices from the 2026 lab-grown market [8, 9].

Product	Substrate	Rate	24 h yield	Value per cycle (2026 wholesale)
Polycrystalline film, set A (inside sheath)	1 m^2, inner-capsule skin	3 µm h^{-1} (1–5)	72 µm; 253 g	—

Product	Substrate	Rate	24 h yield	Value per cycle (2026 wholesale)
Polycrystalline film, set B (outside)	1 m^2, outer wall	3 µm h^{-1} (1–5)	72 µm; 253 g	—
Polycrystalline total	2 m^2		505 g = 2,527 ct	US$ 300,000–3,000,000 as finished thermal-grade plates (50 % usable area, US$ 0.3–3 mm^{-2})
Single-crystal rough	1,000 seeds, 7 × 7 mm	20 µm h^{-1} (10–30)	83 g = 413 ct	US$ 9,081 (rough, US$ 20–25 ct^{-1})
Single-crystal polished equivalent	40 % polishing yield		165 ct	US$ 74,300 (1 ct D–F VS, US$ 350–600 ct^{-1})

3.3 Why the diamond is needed: industrial uses

Polycrystalline CVD diamond is not a substitute for a gemstone; it is an engineering material with a combination of properties no other material offers, and the requirement for it is set by industries that already buy it. Its thermal conductivity, 1500–2200 W m^{-1} K^{-1} for thermal-grade plates (copper: 400), makes it the heat spreader of choice under gallium-nitride and silicon-carbide power transistors, radio-frequency amplifiers and high-power laser diodes; market analyses put the diamond heat-spreader segment at ≈ US$ 0.35 billion in 2025, growing to ≈ US$ 0.75 billion by 2035, with electronics cooling as the largest application [10]. A 1 m^2 film per cycle, diced into 10 × 10 mm plates, is ≈ 5000 heat spreaders per day at 50 % usable area — a meaningful fraction of a market whose bottleneck is exactly the slow, small-area growth of conventional reactors. Second, diamond is the only window material that transmits multi-kilowatt infrared laser beams (10.6 µm CO_2 lasers) without thermal lensing, and it is the standard window and detector material for synchrotron X-ray beamlines. Third, boron-doped diamond is the most robust electrode known — wide potential window, chemically inert, no fouling — and is used for the electrochemical oxidation of persistent organic pollutants in water treatment and for electroanalysis [11]. Fourth, diamond is radiation-hard: diamond detectors monitor beam loss at particle accelerators, and the BEF-2026 gap, with ≈ 7.5×10^{13} photoneutrons per second from the anode, is an environment in which its own product is the appropriate sensor. Fifth, polycrystalline and nanocrystalline diamond coat cutting tools and wire-drawing dies, and nitrogen-vacancy centres in diamond are the working medium of solid-state quantum sensors. Diamond powder from off-specification film has an established cosmetic use in micro-dermabrasion abrasives and diamond-tip exfoliation heads, so that even rejected material has a market.

Table 3 Industrial and cosmetic requirements for CVD diamond and how the apparatus meets them.

Application	Property required	Specification	What BEF-2026 supplies
Heat spreaders (GaN/SiC power electronics, RF, laser diodes)	thermal conductivity	> 1500 W m^{-1} K^{-1}, plates 0.1–0.5 mm, 5–20 mm	polycrystalline film 72 µm per cycle; thicker in multi-cycle runs
High-power laser and X-ray windows	IR transparency, low absorption, strength	optical grade, low nitrogen, polished	requires low-nitrogen growth; feasible with purified H_2/CH_4
Electrochemical electrodes (water treatment, sensing)	boron doping, conductivity	10^{19}–10^{21} B cm^{-3}	add B_2H_6/trimethylboron to the jet
Radiation detectors (accelerators, medical dosimetry)	radiation hardness, charge collection	electronic-grade single crystal	single-crystal seeds; also used inside the apparatus
Cutting tools, wire dies, wear parts	hardness, wear resistance	coatings 5–30 µm	single-cycle films
Quantum sensing (NV centres)	controlled nitrogen, isotopic purity	^{12}C-enriched single crystal	possible with $^{12}CH_4$ feed
Cosmetic abrasives (micro-dermabrasion)	particle hardness, size grading	powder 50–150 µm	milled off-specification film

3.4 Why the diamond is needed: jewellery

Jewellery is the second, and historically the first, reason for growing diamond. Lab-grown gem diamond is now a mature product: single-crystal CVD material is grown on HPHT or CVD seed plates at 900–1200 °C, colour is controlled by nitrogen exclusion or post-growth annealing, and the stones are indistinguishable from mined diamond except by spectroscopy [6, 7]. The market has changed the economics rather than the demand: wholesale prices of polished lab-grown stones fell by 26 % in 2025 and by a further 14 % in the first quarter of 2026, with 1 ct D–F VS stones at US$ 350–600 and CVD rough at US$ 20–25 per carat [8]. Two consequences follow for BEF-2026. First, gem production alone (Table 2: ≈ US$ 74,300 per cycle at polished-equivalent prices, ≈ US$ 9,081 as rough) is worth an order of magnitude less than the thermal-grade film, so the apparatus is an industrial-diamond facility with a jewellery side line, not the reverse. Second, jewellery demand is now driven by volume and by traceability — consumers increasingly ask where a stone was grown — and a large-area, single-site source with an unusual provenance ("grown inside a relativistic energy sheath") is a marketing asset in its own right, independent of the physics. The necessity, in the strict sense, is thus twofold: industry needs the film because nothing else conducts heat as well, and the jewellery trade needs traceable, large-scale, low-cost single-crystal supply.

4 Spacetime Curvature in Brief: the Börekci Metric

The apparatus was motivated by the conjecture that an enclosing near-light-speed energy flow decouples the interior spacetime and transfers to it the time dilation of the flow. The standard theory is unambiguous. In the weak-field limit the metric perturbation is fixed by the energy–momentum tensor of the source; for light and ultra-relativistic particles the tensor is traceless, which doubles the Newtonian source — the classic result of Tolman, Ehrenfest and Podolsky that a beam of light attracts twice as strongly as its energy suggests, while co-directed beams do not interact at all [12, 13, 14]. The active mass of a fast body is $\gamma(1+\beta^2)m \to 2\gamma m$ [15], linear in γ:

$$\nabla^2\Phi = 4\pi G\left(\rho + \frac{3p}{c^2}\right) \;\rightarrow\; \nabla^2\Phi = \frac{8\pi G u}{c^2} \quad (T^{\mu}{}_{\mu} = 0) \tag{3}$$

$$M_{\mathrm{act}} = \gamma(1+\beta^2)\,m \;\rightarrow\; 2\gamma m = \frac{2E}{c^2} \tag{4}$$

We encode the conjecture as a one-parameter deformation of the stationary linearised metric in harmonic gauge, the Börekci metric,

$$ds^2 = -\left(1 + \frac{2(\xi\Phi_s + \Phi_0)}{c^2}\right)c^2dt^2 \;-\; \frac{8\xi}{c}A_i\,dt\,dx^i \;+\; \left(1 - \frac{2(\xi\Phi_s + \Phi_0)}{c^2}\right)\delta_{ij}\,dx^i dx^j \tag{5}$$

$$\Phi_s(\mathbf{x}) = -G\int_{\mathrm{sheath}} \frac{\left[T^{00} + \sum_k T^{kk}\right](\mathbf{x}')}{c^2\,|\mathbf{x}-\mathbf{x}'|}\,d^3x', \qquad \Phi_0(\mathbf{x}) = -G\int_{\mathrm{static}} \frac{\left[T^{00} + \sum_k T^{kk}\right](\mathbf{x}')}{c^2\,|\mathbf{x}-\mathbf{x}'|}\,d^3x' \tag{6}$$

where Φ_s is the potential of the near-light-speed sheath (electrons and laser, with the traceless factor of 2), Φ_0 is the ordinary potential of all static sources (magnet, electrodes, gas, walls, Earth) which enter with unit coupling because the gravitational coupling of static energy is already bounded at the 5×10^{-5} (Kreuzer) and 4×10^{-12} (Bartlett–Van Buren) levels [16, 17], and A_i is the gravito-magnetic potential of the sheath's momentum flux. At $\xi = 1$ Equations (5)–(6) are the standard gravito-electromagnetic metric [18], confirmed

by Gravity Probe B, LARES-2 and optical-clock experiments [19, 20, 21, 22]. The conjecture is parametrised by

$$\xi = 1 + \kappa C(\gamma_s - 1), \qquad 0 \le C \le 1, \qquad \kappa_{\mathrm{GR}} = 0 \tag{7}$$

with C the enclosed fraction of solid angle and κ a coupling to be measured (κ = 0 in general relativity). A clock at rest inside the enclosure has the effective Lorentz factor

$$\Gamma_{\mathrm{in}} \equiv \frac{dt}{d\tau} = \left(1 + \frac{2(\xi\Phi_s + \Phi_0)}{c^2}\right)^{-1/2} \simeq 1 + \frac{\xi|\Phi_s| + |\Phi_0|}{c^2} \tag{8}$$

For BEF-2026 the sheath potential is $\Phi_s/c^2 = -1.27\times10^{-47}$, the static fields give $\Phi_{0,\mathrm{fields}}/c^2 = -5.77\times10^{-37}$ (dominated by the 2 T magnet, with the Laue factor f = 1 for a bound static system), and the wall masses give a static offset of -9.64×10^{-22} (83 attoseconds per day) that is the same whether the sheath is on or off. The conjecture $\Gamma_{\mathrm{in}} = \gamma_e = 49.92$ requires

$$\Gamma_{\mathrm{in}} = \gamma_e \quad \Rightarrow \quad \xi_{L1} \simeq \frac{1 - \gamma_e^{-2}}{2|\Phi_s|/c^2} \tag{9}$$

i.e. $\xi_{L1} = 3.9\times10^{46}$, and a null result with a clock of fractional resolution σ bounds $\xi < \sigma/(|\Phi_s|/c^2)$ (Table 4). The physics behind the smallness of the standard prediction is simply that 7.9×10^{8} electrons, however fast, weigh 7.2×10^{-20} kg; the conjecture is not that this number is wrong but that a completely enclosing flow couples differently, which is precisely what the parameter ξ isolates for measurement. We state plainly that the standard theory predicts no measurable interior time dilation, that the literature on the gravity of light and on gravitational screening [23, 24] weighs against the conjecture, and that the author nonetheless expects a surprising result; the experiment decides.

Table 4 Bounds on the sheath coupling ξ from a null result, and the prediction of the author's conjecture ($\xi_{L1} = 3.9\times10^{46}$). All clocks are compared in the field-on/field-off differential mode, which cancels the static wall-mass term.

Instrument	Resolution σ	Excludes (null result)	Conjecture (L1) predicts
Chip-scale atomic clock, 24 h	10^{-12}	$\xi > 7.8\times10^{34}$	23 h 31 min offset
Optical clock (laboratory class)	10^{-18}	$\xi > 7.8\times10^{28}$	23 h 31 min offset
Diamond chemical clock (Section 5)	$\delta r = 1\times10^{-3}$ in thickness ratio	$\xi > 7.8\times10^{43}$	thickness ratio 0.020
General relativity (ξ = 1)	—	—	sheath offset 1.1×10^{-42} s per day

5 Diamond Yield under the Börekci Metric: the Chemical Clock

A CVD film integrates a chemical rate over the proper time of its substrate. If the interior of the enclosure runs slow by the factor Γ_{in} of Equation (8), substrate set A (on the capsule skin, inside the sheath) accumulates less material per external day than set B (on the outer wall, outside the sheath), everything else — gas, temperature, hydrogen flux — being equal by construction. The thickness ratio is therefore a direct reading of the metric:

$$r \equiv \frac{t_{\mathrm{in}}}{t_{\mathrm{out}}} = \frac{1}{\Gamma_{\mathrm{in}}} = \sqrt{1 + \frac{2(\xi\Phi_s + \Phi_0)}{c^2}} \simeq 1 - \frac{\xi|\Phi_s|}{c^2}, \qquad \xi < \frac{\delta r}{|\Phi_s|/c^2} \tag{10}$$

This is a clock without electronics, immune to electromagnetic pickup from the 25 MV system, and it can be read after the run with an interferometer or a stylus profilometer to a relative precision of 10^{-3} once the two sets are cross-calibrated by swapping their positions in a control cycle. Table 5 and Figure 2 give the yield of set A as a function of ξ. In general relativity the two sets differ only by the static potential difference between their positions ($\approx 10^{-22}$, from the wall masses); the sheath itself contributes 10^{-47}. The conjecture predicts that set A grows only 5.1 g against 253 g on set B — a ratio of 0.020 that no calibration error could mimic. A null result at $\delta r = 1\times10^{-3}$ bounds $\xi < 7.8\times10^{43}$; this is far weaker than the optical-clock bound, but it is an independent bound from an entirely different physical channel, and it excludes the conjecture by a margin of 500 in ξ. Two subtleties are recorded. First, the sheath does not intercept the gas or the hydrogen flux (its density is 6.1 cm^{-3} and its collisionless skin depth $\approx$ 2.1 km), so set A is chemically equivalent to set B in the standard theory. Second, the growth on set A is also exposed to the sheath's photons; the control cycle with the sheath on but the capsule potential removed (electrons diverted to a dump) separates radiative from metric effects.

Table 5 Diamond yield on the inside substrate set as a function of the sheath coupling ξ (set B fixed at 253 g); Γ_{in} includes the sheath and the static field terms, while the static wall-potential difference between the two positions ($\approx 10^{-22}$) is omitted. The last row is the author's conjecture; the chemical-clock bound is $\xi < 7.8\times10^{43}$.

ξ	Γ_{in}	Thickness ratio $r = t_A/t_B$	Set A yield (g / 24 h)	Total yield (g / 24 h)
1	$1 + 5.8\times10^{-37}$	$1 - 5.8\times10^{-37}$	252.7	505.4
1.0×10^{10}	$1 + 7.0\times10^{-37}$	$1 - 7.0\times10^{-37}$	252.7	505.4
1.0×10^{20}	$1 + 1.3\times10^{-27}$	$1 - 1.3\times10^{-27}$	252.7	505.4
1.0×10^{30}	$1 + 1.3\times10^{-17}$	$1 - 1.3\times10^{-17}$	252.7	505.4
1.0×10^{40}	$1 + 1.3\times10^{-7}$	$1 - 1.3\times10^{-7}$	252.7	505.4
1.0×10^{43}	1.0001	0.9999	252.7	505.4
1.0×10^{44}	1.0013	0.9987	252.4	505.1
1.0×10^{45}	1.0130	0.9872	249.5	502.2
1.0×10^{46}	1.1585	0.8632	218.1	470.9
3.9×10^{46}	49.9238	0.0200	5.1	257.8

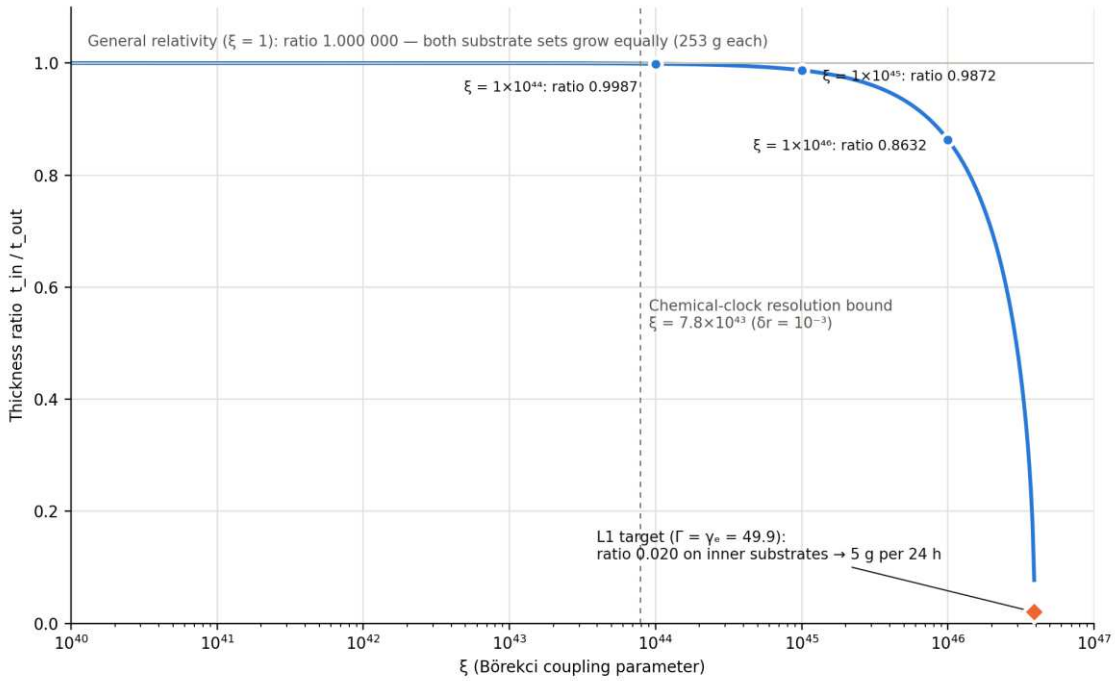


Fig. 2 The diamond chemical clock: thickness ratio of the inside (set A) to the outside (set B) film as a function of the sheath coupling ξ. The shaded band is the assumed resolution $\delta r = 10^{-3}$; the dashed line is the corresponding bound on ξ; the orange marker is the author's conjecture ($\Gamma_{in} = \gamma_e = 49.9$, ratio 0.020). General relativity sits at ξ = 1, far off the left edge of the plot, with a ratio deviating from unity by $\approx 10^{-22}$ (static wall-potential difference between the two positions, omitted in the plot) and by 10^{-47} from the sheath.

6 Antimatter Production in Brief

The 25 MeV electrons stopping in the tungsten–rhenium anode radiate 0.44 of their energy as bremsstrahlung [25], and photons above 1.022 MeV convert to electron–positron pairs in the nuclear Coulomb field — the Bethe–Heitler process [26]. Geant4 studies of tantalum/tungsten converters give a forward fast-positron yield of 1.4×10^{-2} e^+/e^- at 20 MeV and 6.1×10^{-2} at 40 MeV at the optimum thickness of ≈ 1 radiation length [27]; we take 2.3×10^{-2} at 25 MeV and recommend a 4 mm converter plate on the anode face, since the 20 cm solid anode of the original design (57 X_0) would let only $\approx 1\times10^{-3}$ escape.

$$N_{e^+} = Y(E_0, t)\frac{I t_{\mathrm{run}}}{e}, \qquad Y(25\ \mathrm{MeV},\ \approx 1X_0) \simeq 2.3\times10^{-2} \tag{11}$$

Table 6 Positron production and radiological figures per 24 h cycle.

Quantity (2 mA, 24 h)	Value	Remark
Electrons delivered	1.08×10^{21}	1.25×10^{16} s^{-1}
Fast positrons leaving a 4 mm converter	2.5×10^{19} (22.6 ng)	world-class flux: 2.9×10^{14} e^+ s^{-1}
Pairs created inside a thick anode	5.4×10^{20}	annihilate in situ; 1.1×10^{21} photons of 511 keV
Species	e^+ only (transient positronium)	no antiprotons (threshold 5.6 GeV), no antimuons (211 MeV)
Slow positrons after moderation (10^{-3}) and trapping (20 %)	5.7×10^{10} s^{-1}	record single-trap capacity 4×10^9 [28]
Storable in 100 traps × 10^{11}	1×10^{13} (9 fg)	fills in 174 s; storage, not production, is the bottleneck
Monetary value of the daily output	≈ US$ 565	at US$ 25 billion g^{-1} [29]
Photoneutrons from the anode	7.5×10^{13} s^{-1}	activation of anode and walls; test subject dose 2.2×10^{-13} Sv per 24 h

Two conclusions matter for the present paper. The positron flux, $\approx 2.9\times10^{14}$ e^+ s^{-1}, is comparable with the strongest linac-based positron sources [30] and is a genuine scientific asset; but its monetary value (US$ 565 per day) is negligible next to the diamond, and the pairs cannot be stored — they must be used as a continuous beam. The figure of 542 ng h^{-1} in the first preprint [1] violated energy conservation and is superseded. The 3.1 m wall shields the inner cavity to 2.2×10^{-13} Sv per cycle, so the biological experiments envisaged in the cavity are radiologically safe; the diamond substrates in the gap are not, and set A must be shadowed from the direct anode line of sight.

7 Discussion

Falsifiability. The apparatus produces two clocks, one atomic and one chemical, and each yields either a measurement of ξ or a bound. The atomic clock is the more sensitive by thirty orders of magnitude; the chemical clock is the more robust, because a diamond film cannot be disturbed by the electromagnetic environment of a 25 MV discharge, and because its reading is a physical object that can be re-measured by any laboratory. A ratio of 0.020 between two 1 m^2 films is not a subtle effect. The author's conjecture is therefore not protected by experimental difficulty: if it is wrong, the films will say so on the first cycle.

Objections. Three results in the literature weigh directly against $\xi \gg 1$. The gravity of light is known exactly and co-directed beams do not interact [12, 13, 14], so the sheath's effect on its interior is fixed by its energy — -1.27×10^{-47}. The positive-mass theorem forbids complete angular gravitational screening in vacuum, allowing localisation only in cones [23]; the sheath is designed to enclose all directions. The equivalence principle holds to 10^{-15} [24] and active–passive mass equivalence to 4×10^{-12} [17], so any anomalous coupling must hide in the dynamic, enclosing, near-light-speed character of the flow that these static tests do not probe. Earlier claims of gravitational shielding with superconductors were not reproduced [31, 32], which is why the protocol prescribes blind analysis, field-on/field-off differentials and position-swapped control cycles for the films.

What is gained either way. If $\xi = 1$, the apparatus is a large-area diamond reactor of unusual hydrogen chemistry (beam-dissociated, filament-assisted) producing $\approx$ 2,527 carats of thermal-grade film and $\approx$ 413 carats of single-crystal rough per cycle, plus a continuous positron beam, and it sets the first laboratory bound on the gravitational coupling of an enclosing near-light-speed energy flow. If $\xi \gg 1$, the diamond films are the first material objects to record engineered time dilation. The author states his expectation of the second outcome; the standard theory, and the literature, expect the first.

Limitations. This is a pre-experimental study; the diamond growth rates are taken from conventional reactors and the beam-assisted chemistry has not been demonstrated at this scale; the yields of Table 2 are nominal within a factor of three. The metric is linearised, and a confirmed $\xi \gg 1$ would require a non-linear theory that this paper does not offer. The engineering of the electron sheath (its transport around the capsule, the 25 MV vacuum gap, the cooling of the rotating anode) is unsolved and is treated in the technical report. Prices of lab-grown diamond are volatile; the value figures are indicative.

8 Conclusions

BEF-2026 makes diamond. With CH_4/H_2 chemistry, a beam-heated tungsten–rhenium anode and two 1 m^2 substrate sets, it yields $\approx$ 505 g (2,527 carats) of polycrystalline thermal-grade film per 24 h cycle — material required by power electronics, laser optics, electrochemistry and detector physics — and $\approx$ 413 carats of single-crystal rough for jewellery, a market that needs traceable large-scale supply more than it needs new sources of price. The film is also a clock. Under the Börekci metric, whose single parameter ξ multiplies the potential of the enclosing sheath and reduces to general relativity at $\xi = 1$, the ratio of the

film thicknesses inside and outside the enclosure equals $1/\Gamma_{in}$: general relativity predicts unity to one part in 10^{21}, a ratio resolution of 10^{-3} bounds $\xi < 7.8\times10^{43}$, and the author's conjecture predicts 0.020. Positron production (≈ 22.6 ng per day, e^+ only) is scientifically significant and economically negligible. The paper thus offers a proposal in which the same object — a diamond film — is the product, the instrument and the verdict.

Statements and Declarations

Funding. The work was financed entirely by the author; no funding was received from any person, institution, organisation or company. **Competing interests.** The author has filed a patent application for the Börekci Energy Field – spacetime dilation and antimatter production system; the diamond-production configuration described here is part of that application. He declares no other financial or non-financial competing interests. **Ethics approval.** No experiments involving humans or animals were performed; the animal component of the full apparatus (a test subject in the inner cavity) is not part of this paper and would require ethics-committee approval. **Data availability.** All numerical results are generated by the calculation model provided as Online Resource 1 (Python source and JSON output); no other data were generated. **Author contributions.** H.B. conceived the apparatus, the hypothesis and the diamond chemical-clock proposal, and wrote and approved the manuscript. **Use of generative AI.** A large language model (Claude, Anthropic) was used, under the author's direction, for the numerical calculations, literature retrieval and verification, figure preparation and language editing; all references and numbers were checked by the author, who takes full responsibility for the content.

References

[1] Börekci H. A near-light-speed enclosing energy field as a positron source and candidate time-dilation capsule. *Research Square* preprint v1, posted 30 June 2026. https://doi.org/10.21203/rs.3.rs-9999735/v1

[2] Koyanagi T, Katoh Y. Thermal properties of SiC/SiC composites for fusion applications. ORNL report ORNL/TM-2018 (Pub117983), Oak Ridge National Laboratory, 2018.

[3] Concept Alloys. Tungsten–rhenium (W-25Re / W-26Re) alloy data sheet: density 19.7 g/cm^3, melting point 3120 °C, tensile strength 1380 MPa (RT) / 165 MPa (2000 °C).

[4] Krätschmer W, Lamb LD, Fostiropoulos K, Huffman DR. Solid C_{60}: a new form of carbon. *Nature* **347**, 354–358 (1990). https://doi.org/10.1038/347354a0

[5] Angus JC, Hayman CC. Low-pressure, metastable growth of diamond and 'diamondlike' phases. *Science* **241**, 913–921 (1988). https://doi.org/10.1126/science.241.4868.913

[6] Tallaire A, Achard J, Silva F, Brinza O, Gicquel A. Growth of large size diamond single crystals by plasma assisted chemical vapour deposition: recent achievements and remaining challenges. *Comptes Rendus Physique* **14**, 169–184 (2013). https://doi.org/10.1016/j.crhy.2012.10.008

[7] Yan CS, Vohra YK, Mao HK, Hemley RJ. Very high growth rate chemical vapor deposition of single-crystal diamond. *Proceedings of the National Academy of Sciences* **99**, 12523–12525 (2002). https://doi.org/10.1073/pnas.152464799

[8] Golan E. Lab-grown diamond wholesale prices fall 14 % in Q1 2026. AIDI / Edahn Golan Diamond Research report (2026); Draco Diamond, Lab diamond price trend report 2020–2026.

[9] MSE Supplies. Polycrystalline CVD diamond wafer 10×10×0.3 mm, thermal grade (1500 W m^{-1} K^{-1}) — catalogue price (2026).

[10] Roots Analysis. Diamond heat spreaders market: industry trends and global forecasts to 2035 (2025 edition). https://www.rootsanalysis.com/diamond-heat-spreaders-market

[11] Macpherson JV. A practical guide to using boron doped diamond in electrochemical research. *Physical Chemistry Chemical Physics* **17**, 2935–2949 (2015). https://doi.org/10.1039/C4CP04022H

[12] Tolman RC, Ehrenfest P, Podolsky B. On the gravitational field produced by light. *Physical Review* **37**, 602–615 (1931). https://doi.org/10.1103/PhysRev.37.602

[13] Bonnor WB. The gravitational field of light. *Communications in Mathematical Physics* **13**, 163–174 (1969). https://doi.org/10.1007/BF01645484

[14] Faraoni V, Dumse RM. The gravitational interaction of light: from weak to strong fields. *General Relativity and Gravitation* **31**, 91–105 (1999). https://doi.org/10.1023/A:1018867405133

[15] Olson DW, Guarino RC. Measuring the active gravitational mass of a moving object. *American Journal of Physics* **53**, 661–663 (1985). https://doi.org/10.1119/1.14280

[16] Kreuzer LB. Experimental measurement of the equivalence of active and passive gravitational mass. *Physical Review* **169**, 1007–1012 (1968). https://doi.org/10.1103/PhysRev.169.1007

[17] Bartlett DF, Van Buren D. Equivalence of active and passive gravitational mass using the Moon. *Physical Review Letters* **57**, 21–24 (1986). https://doi.org/10.1103/PhysRevLett.57.21

[18] Mashhoon B. Gravitoelectromagnetism: a brief review. In: Iorio L (ed.) *The Measurement of Gravitomagnetism: A Challenging Enterprise*, Nova Science, New York, 2007, pp. 29–39; arXiv:gr-qc/0311030.

[19] Everitt CWF et al. Gravity Probe B: final results of a space experiment to test general relativity. *Physical Review Letters* **106**, 221101 (2011). https://doi.org/10.1103/PhysRevLett.106.221101

[20] Ciufolini I et al. LARES-2 satellite measures frame-dragging effect around the Earth. *Nature* **655**, 332–335 (2026). https://doi.org/10.1038/s41586-026-10715-0

[21] Chou CW, Hume DB, Rosenband T, Wineland DJ. Optical clocks and relativity. *Science* **329**, 1630–1633 (2010). https://doi.org/10.1126/science.1192720

[22] Bothwell T, Kennedy CJ, Aeppli A, Kedar D, Robinson JM, Oelker E, Staron A, Ye J. Resolving the gravitational redshift across a millimetre-scale atomic sample. *Nature* **602**, 420–424 (2022). https://doi.org/10.1038/s41586-021-04349-7

[23] Le Floch B, LeFloch PG. Optimal shielding for Einstein gravity. *Classical and Quantum Gravity* **41**, 13LT02 (2024). https://doi.org/10.1088/1361-6382/ad5137

[24] Touboul P, Métris G, Rodrigues M, Bergé J, Robert A, et al. (MICROSCOPE Collaboration). MICROSCOPE mission: final results of the test of the equivalence principle. *Physical Review Letters* **129**, 121102 (2022). https://doi.org/10.1103/PhysRevLett.129.121102

[25] Berger MJ, Coursey JS, Zucker MA, Chang J. ESTAR: stopping powers and ranges for electrons (NIST Standard Reference Database 124). National Institute of Standards and Technology. https://physics.nist.gov/PhysRefData/Star/Text/ESTAR.html

[26] Bethe H, Heitler W. On the stopping of fast particles and on the creation of positive electrons. *Proceedings of the Royal Society A* **146**, 83–112 (1934). https://doi.org/10.1098/rspa.1934.0140

[27] O'Rourke BE, Hayashizaki N, Kinomura A, Kuroda R, Minehara EJ, Oshima N, Suzuki R, Toyokawa H. Simulations of slow positron production using a low-energy electron accelerator. *Review of Scientific Instruments* **82**, 063302 (2011); arXiv:1102.1220. https://doi.org/10.1063/1.3600899

[28] Fitzakerley DW et al. (ATRAP Collaboration). Electron-cooled accumulation of 4×10^9 positrons for production and storage of antihydrogen atoms. *Journal of Physics B* **49**, 064001 (2016). https://doi.org/10.1088/0953-4075/49/6/064001

[29] NASA (Steigerwald B). New and improved antimatter spaceship for Mars missions. NASA feature, 14 April 2006 (positron cost estimate of G. A. Smith, Positronics Research LLC, NIAC study).

[30] Danielson JR, Dubin DHE, Greaves RG, Surko CM. Plasma and trap-based techniques for science with positrons. *Reviews of Modern Physics* **87**, 247–306 (2015). https://doi.org/10.1103/RevModPhys.87.247

[31] Hathaway G, Cleveland B, Bao Y. Gravity modification experiment using a rotating superconducting disk and radio frequency fields. *Physica C* **385**, 488–500 (2003). https://doi.org/10.1016/S0921-4534(02)02284-0

[32] Lörincz I, Tajmar M. Null-results of a superconducting gravity-impulse-generator. AIAA Paper 2016-4988, AIAA Propulsion and Energy Forum (2016). https://doi.org/10.2514/6.2016-4988

Supplementary Files

This is a list of supplementary files associated with this preprint. Click to download.

- ESM1calculationmodel.zip